RESEARCH ARTICLE

Partial Discharges Acceptance Criteria for AC Rotating Machines Insulation Systems

ALFREDO CONTIN [ID] **[1], (Life Member, IEEE), AND ANDREA PICCOLO[2]**
[1]Department of Engineering and Architecture, University of Trieste, 34127 Trieste, Italy
[2]Department of Asset Management, DNV Energy Systems, 6812 Arnhem, The Netherlands

Corresponding author: Alfredo Contin (contin@units.it)

ABSTRACT A new pass/fail criterion based on the shape analysis of phase-resolved Partial Discharges (PRPD) patterns is proposed in this study to overcome the problems generated by the use of partial discharge (PD) amplitude threshold levels. Insulation systems based on mica tapes are considered to be in good condition when they are affected only by distributed micro-void PD and no other type of defect incept discharges. This definition implies the possibility of discriminating between PRPD patterns owing to different defect typologies. With this approach, the diagnostic information includes the defect typology that affects a specific insulation component, not the PD amplitude. Consequently, the PRPD pattern must address the same defect typology because the defect remains the same even if different PD instruments and couplers are used while testing different insulation systems and under different test conditions. A wide number of PRPD patterns associated with well-known defect typologies are presented and discussed in this paper to empirically demonstrate that the PRPD patterns associated with distributed micro voids are clearly distinguishable from the other PRPD patterns. Significant applications of the method in the condition assessment of the insulation system of coils, bars, and complete machines are discussed, highlighting the important role played by the separation phase prior to the identification of defects.

INDEX TERMS Acceptance test, condition assessment, insulation diagnostics, partial discharges, rotating machines.

I. INTRODUCTION

Partial Discharges (PD) are widely used in acceptance tests of new coils, bars, or complete machines, and in the condition assessment of insulation systems for AC stator windings, [1], [2], [3], [4]. Even though it is extensively applied, there is no clear agreement regarding the interpretation of PD test results. The pass/fail criteria based on amplitude threshold levels are still widely used. Although they are attractive for their ease of interpretation, threshold acceptance levels may lead to incorrect decisions. This observation is justified by the fact that different defects can be simultaneously active during each acquisition time, and the PD amplitude can change over time owing to discharge-site conditioning or defect evolution. Moreover, different defect typologies can have different impacts on the insulation system reliability, and it is not possible to distinguish them by considering only the PD amplitude.

The associate editor coordinating the review of this manuscript and approving it for publication was Ali Raza [ID].

In addition, a low PD amplitude does not necessarily indicate that the insulation is in good conditions, [5]. It is also known that different PD instruments could not provide comparable results in terms of signal amplitudes owing to the different dynamic characteristics of both instruments and couplers, or the different locations of the defect [6].

Currently, the identification of PD sources (defects) is usually made by experts who rely mainly on the visual evaluation of the PRPD patterns ([7]) with the implicit assumption that there is a direct correlation between the pattern shapes and defect typologies. Examples of PRPD patterns owing to typical PD activities occurring in rotating machine stator windings are reported in the Annexes of both IEEE-1434 ([2]) and IEC-60034-27 ([3], [4]).

The purpose of this paper is to show how the shape analysis of PRPD patterns can be used in acceptance tests of new insulation systems during PD monitoring or diagnostic tests instead of the PD amplitude threshold levels. An insulation system based on mica tapes is considered

to be in good condition when it is affected only by PD occurring in micro-voids distributed within the ground-wall insulation and no other PD due to different defect typologies, is detected during the test. Therefore, the test fails when PRPD patterns address to other types of defects. A proper signal separation procedure that can split the experimental pattern into sub-patterns that are pertinent to a specific noise or defect typology is a fundamental tool to allow the use of the proposed method, [8], [9], [10], [11]. To be generally applicable, the new pass/fail criterion must provide the same result when different PD instruments and couplers are used, as well as when considering different insulation systems and different test conditions. A wide set of defect typologies and the relevant PRPD patterns obtained by testing new or aged coils, bars, and complete machines, with or without artificial defects, were analyzed to validate the test and complete the list of patterns presented in [2], [3], and [4]. Practical examples are discussed in this paper to demonstrate the significant improvements achieved by applying the proposed approach.

In this paper, the attention is addressed only to the relationship between PRPD patters and defect typologies and not to the relevant harmfulness (see e.g., Table E.1.2 of Annex E, IEC 60034-27-1). Once the defect is identified, the time behavior of PD magnitude (average or maximum) and repetition rate referred to the specific defect and obtained using the same PD instrument and coupler, can help in maintenance planning.

II. THE TESTED INSULATION SYSTEMS
The proposed pass/fail criterion was developed by analyzing a very large set of PRPD patterns recorded in a timeframe of many years and testing different insulation systems designed for rated voltages in the range of 4–18 kV, classes F and H. In particular:

- Resin-Rich Technology (RR): Roebel bars of different lengths and thicknesses, manufactured with materials from two providers (RR-1 and RR-2), designed for voltage ratings of 11 kV and above, completed with polyester-graphite varnish as Conductive Slot Coating (CSC) and Silicon Carbide (SiC)-polyester varnish as Stress Control Coating (SCC).
- Porous microtape insulation (PTI): Different types of coils and complete machines provided ground-wall insulation based on a two-layer tape (mica-paper and non-woven fiberglass). Polyester-graphite tapes (above 4.5-5 kV) and SiC polyester tapes (above 6-6.5 kV) were used as the CSC and SCC, respectively. Most of these coils are equipped with additional thermosetting sealing tapes on the overhangs. Coils and complete machines were impregnated with polyester-imide resin using Global Vacuum Pressure Impregnation (GVPI) techniques. Even with this insulation technology, coils and stator windings were realized using materials from two different suppliers (PTI-1 and PTI-2).

- Four-Layer Mica-Tapes (FLT): Different types of coils and complete machines whose ground-wall insulation is based on a four-layer tape (mica-paper, non-woven fiberglass, and thin polyester film on both sides of the tape). Above of about 4.5-5 kV, a polyester-graphite tape was used as the CSC while from to 6-7 kV and above, a SiC-polyester tape was adopted as the SCC. Epoxy resin was used for impregnation of both coils and complete machines using the GVPI technique.

New bars and coils were tested mainly in the laboratory, whereas new stators or complete machines were tested in the factory during the acceptance tests. Aged bars and coils were evaluated in the laboratory during the multifactor aging tests. The service machines were tested on-line or off-line during their periodic maintenance.

Tests were also performed using bars/coils provided by artificially reproduced defects, while tests with multiple bars inserted in a stator mock-up were performed to simulate different positions of the defects along the winding [5], [12], [13].

Only PRPD patterns due to well known defects were considered in this investigation.

III. PD TEST SET-UP AND EVALUATION
Four different commercial PD instruments with an amplitude scale variable from 2mV up to 5V or 20V and frequency bandwidths ranging from 3 MHz to 25-200 MHz of high cut-off, connected to different coupling capacitors, C_k, (100pF, 500pF, 1nF, 2nF), were used in the PD tests. A high-frequency current transformer (HFCT) with a flat bandwidth up to 80 MHz and an antenna probe integrated in a fully portable PD instrument (bandwidth of 100 MHz) able to simultaneously record both PD and voltage reference, ([15]) were also used to record PD pulses. Coupling capacitors were connected to different detection impedances to obtain different bandwidths for the acquisition system (3, 10, 25, 50, 100, and 200 MHz). This variety of instrumentation allows empirical verification of the robustness of pattern shapes. It should be noted that the real bandwidth of the test circuit is due to the dynamic characteristics of the transmission path between the discharge site and the detection point and does not necessarily correspond to the dynamic characteristics of the signal acquisition system. The trigger level has been selected to eliminate as much as possible the influence of the noise but preserving the diagnostic information provided by the shape of the PRPD pattern.

The PD offline test procedure remains the same as that indicated in [2] and [3]. The PD inception voltage is first determined by continuously increasing the applied voltage, followed by a period of voltage conditioning. Finally, the PD extinction voltage is recorded by decreasing the voltage. Then, the test voltage is increased step-by-step from an initial value (e.g., close to the PDIV) up to the maximum voltage level established according to, for example, par.9.1.5 "Test Voltages", [3]. For the stator and complete machines, tests

were performed up to $1.2U_0$ (U_0 is the rated phase-to-ground voltage).

Different signal separation procedures have been proposed to verify the simultaneous presence of noise or PD signals, but only a few have been implemented in commercial PD instruments (see e.g., [8], [9], [15]). In general, separation refers to the classification of the recorded signals in groups by assuming that different PD sources and pulsating noise, are characterized by different waveforms.

The examples discussed in the paper refer to the use of the TF-Map. The acquired waveforms are mapped in a two-dimensional space obtained evaluating the time and frequency spectrum ''center gravity'' of each recorded signal. Thus all the pulses are mapped in a space ''number of pulses as a function of the equivalent time (T) and equivalent frequency (F) where the information provided by the signal shape is preserved, [8]. Clusters containing signals having similar shapes are grouped together while pulses having different shape are mapped in different areas of the map. Different clustering algorithms can be used to separate the different groups of signals and specific pointers allow to reconstruct the sub-patters associated to each single group. Because separation plays a very important role in this test method, the separation map should be included in the test report to highlight the presence of sub-patterns within the acquired PRPD pattern. PRPD sub-patterns due to pulsating noise can be easily recognized and rejected, [12].

Currently, two methods can be used to analyze the PRPD patterns:

A) By comparison of the experimental PRPD patterns with those used as a reference where the association between patterns and defect typology is well established. Annex A of [2] and Annex B of [3] show some reference patterns relevant to specific defects to be used for the comparison but these list are incomplete and these reference patters were obtained by testing mainly resin-rich bars provided by varnisched CSC and SCC, and no other insulation technologies have been considered. This study intends to fill this knowledge gap.

B) by PRPD pattern shape analysis summarized as follow, [7]:
  - The dominant PD polarity is selected in terms of symmetry/asymmetry of higher amplitude and repetition rate with respect to the polarity of the voltage half-cycle.
  - Evaluate the symmetry/asymmetry of the dominant PRPD half-pattern with respect to the phase angle of the applied voltage (symmetry in phase or left/right-skewed dominant half-pattern).
  - Evaluate the geometrical profile of the dominant PD half-pattern.

Method B) is here adopte to evaluate the PRPD shapes.

IV. PRPD PATTERNS DUE TO DISTRIBUTED MICRO-VOID PD

As a matter of fact of RR or GVPI/VPI insulation technologies, gas-filled pockets with sizes in the range of few up to hundreds microns always remain embedded within the ground wall owing to the impossibility of the impregnation resin to fill all the voids between tape-layers or between adjacent turns [16], [17], [22]. When the local electric field is sufficiently high, PD occurs in these voids (distributed micro-void PD), but this PD activity has negligible effects on the insulation owing to the presence of mica, which constitutes a physical barrier for discharge growth. Thus, this type of discharge is normally present during machine service, and the PRPD patterns associated with this type of defect can be used as a reference to establish the good conditions of the insulation.

On this basis, an insulation system can be defined in good condition if it is affected by distributed micro-void PD and no discharges due to other types of defect typologies are present. Therefore, the first step of this analysis is the recognition of PRPD patterns owing to discharges in distributed microvoids.

A. NEW INSULATION SYSTEMS

The PRPD patterns recorded by testing the new insulation systems in good conditions at the first application of the voltage, are composed of a mix of low- and high-amplitude discharges. A combination of streamer and Townsend discharges can occur inside voids depending on the thermodynamic conditions (temperature and pressure) of the internal gases, sizes, and state of the cavity surface, [18], [19], [20], [21]. Figure 1 shows results of PD tests performed to evaluate the manufacturing quality of a complete coil rated 11 kV and insulated using the PTI-1 system. The PD inception voltage was approximately 4.7 kV. PD tests were performed applying voltages from 5 kV up to 11 kV with steps of 1 kV using a $C_k = 1$ nF and a commercial PD instrument with a system bandwidth of 30 MHz. The PRPD patterns obtained at 6, 8, 10, and 11 kV are shown in Figures.1A, 1B, 1C, and 1D, respectively. As can be seen, all the PRPD patterns are characterized by rounded stripes of larger discharges plus a rounded base of low-amplitude PD.

This type of pattern can be justified by considering patterns recorded by testing single voids embedded in solid dielectrics (see e.g., [18], [19], [20], [21]). These experiments showed that a PRPD pattern symmetric in voltage polarity and composed of both high- and low-amplitude discharges was initially recorded (called ''rabbit-like'' PD pattern, [21]), during which a decrease in both the amplitude and repetition rate of the high-amplitude discharges was observed, while the low-amplitude PD increased mainly in the repetition rate. At the end of the conditioning period, the higher discharges disappear and the PD pattern shows rounded and symmetric shape (called ''turtle-like'' PD pattern, [21]).

The TF-Map has been used to verify the presence of additional PD phenomena (Figure 2). Both maps relevant to
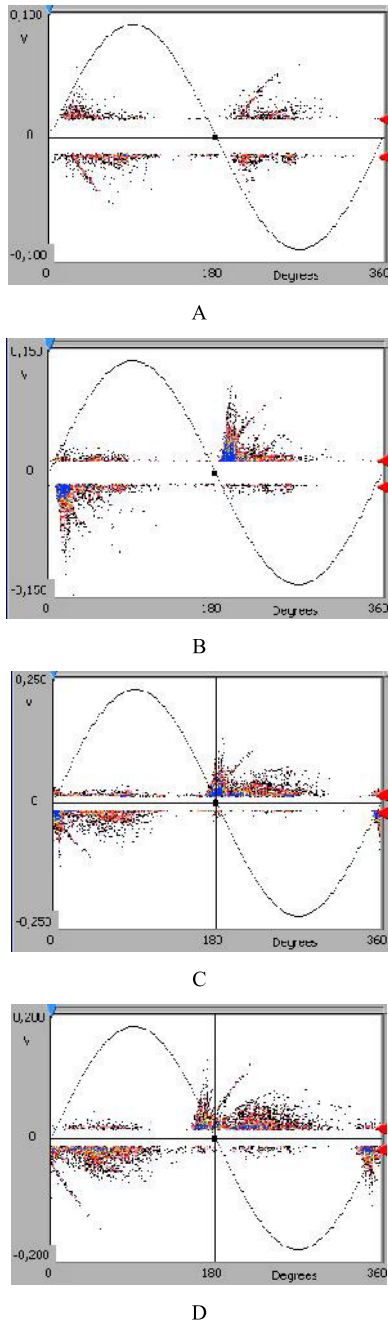
FIGURE 1. PRPD patterns recorded testing a coil rated 11 kV, insulated with the PTI-1 system, at different voltage levels. PRPD patterns recorded at A) 6 kV; B) 8 kV; C) 10 kV; D) 11 kV.
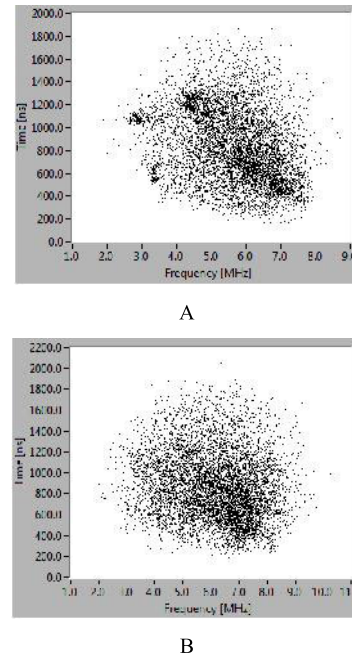

FIGURE 2. Examples of TF maps derived from PD signals recorded at A) 6 kV and B) 11 kV and relevant to PRPD patterns of Figures 1A and 1D, respectively.

bility of these results. The results are shown in Figure 3. In particular, Fig.3A shows a PRPD pattern recorded by testing a new coil at 6.36 kV (phase-to-ground rated voltage) insulated with FLT type.

The PRPD pattern recorded by testing a complete machine rated 13 kV at 7.5 kV and insulated with the PTI-1 system is shown in Fig.3B. The coil surfaces were protected using polyester tape. Fig.3C and 3D show PRPD patterns recorded during the qualification tests of coils used later to form the windings of the machine in Fig.3B at their phase-to-ground rated voltage (PTI-1 insulation type). In particular, pattern of Fig.3C has been recorded using a commercial PD instrument having a bandwidth of 30 MHz, connected to a $C_k = 500$pF, while an antenna-based instrument (bandwidth of 100 MHz) was used to test the same coil at the same voltage whose pattern has been reported in Fig.3D. The diagnostic information provided by these patterns is the same even when different setups are used and different PD amplitudes were recorded.

Based on these results, the insulation systems of the tested coils and machines were considered in good condition and passed the proposed PD test.

B. LOW QUALITY IMPREGNATION

Bad coil taping or low-quality impregnation due to incorrect curing processes can generate larger micro-void inclusions within the ground-wall insulation or between adjacent turns.

During tests performed to qualify new insulation systems for ac rotating machines rated 6.8 – 18 kV, PD measurements were performed on some coils provided by PTI-1 insulation. Small samples of their main insulation were removed
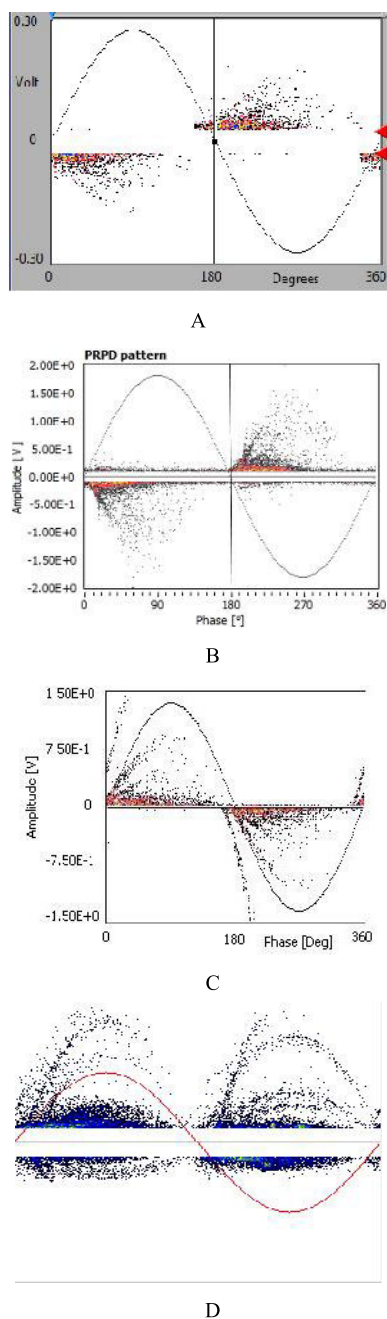
PRPD patterns recorded at 6 kV (Fig.2A) and 11 kV (Fig.2B) were characterized by a single group of signals, and no other groups were found.

A large number of PD tests performed to evaluate the initial conditions of different types of insulation systems provided the same results. PD tests were performed using different instruments and couplers (different gains and bandwidths) at different voltage levels or with defects in different locations to verify the robustness of the PRPD patterns and the repeata-

A

B

C

D

FIGURE 3. PRPD patterns recorded testing (A): a single coil at 6.38 kV (phase-to-ground), insulated with FLT technology; (B): a single phase of a complete stator insulated with PTI-1 system; (C): a complete coil at 6.38 kV insulated with PTI-1; (D) the same coil of Fig.3C but using an antenna probe.

and examined using the X-Ray Computed Tomography to virtually reconstruct the void content embedded within the insulation, [17], [22].

The void density and the distribution of the void sizes associated with the PRPD patterns recorded testing the same coil, evidenced a potential correlation between the void sizes and the thickness of the "stripes" of higher PD that appeared in the PRPD pattern: larger are the void sizes, larger is the

thickness of these stripes. A PRPD pattern obtained testing a PTI-1 insulated coil with high content of larger void inclusions is reported in Figure 4A. The impregnation parameters (temperature, pressure, resin viscosity) were modified until an acceptable void content has been obtained. Examples of PRPD patterns recorded testing coils with reduced void content have been discussed in Par.IV.A and shown in Figures 1 and 3.

PRPD patterns recorded testing new coils insulated with PTI-2 technology in two different laboratories and using two different commercial PD instruments (the second provided by an input logarithmic amplifier), shown similar shapes. Figures 4B and 4C reports examples of PRPD patterns recorded at the same voltage level. As can be seen, both patterns shows larger high-amplitude PD stripes if compared with those reported in Figures 1 and 3 of this paper. Coils were cut and examined at the microscope and the images evidenced the presence of voids due bad taping not filled by the impregnation resin.

The assumption that larger are the void sizes, larger is the thickness of these stripes has been verified by looking at investigations dealing with PD incepted in calibrated voids having different sizes and shapes, [18], [19], [20], [21]. The potential correlation between void sizes and the thickness of the higher discharges collected in the PRPD pattern (the so called "rabbit ear" PD, [21]), found evidence.

Figure 4D refers to PD tests performed off-line on a single phase of an induction motor rated 11 kV and insulated using the FLT technology. This example is to show that this results find evidence even in complete machines that adopted a different insulation technology.

It must be point out, that this type of PRPD patterns can be associated to distributed micro-void PD which have a negligible effect on the insulation reliability.

During tests performed to evaluate the quality of the impregnation process described above, PRPD patterns similar to those reported in Figure 5 and characterized by a single, large stripe of high-amplitude discharges were found (macro-void). This characteristics allows to distinguish distributed micro-voids and a single macro-void. For example, Figs.5A and 5 B show patterns recorded at 7.2 kV using $C_k = 1nF$ and a HFCT, respectively. Again, the use of X-Ray CT allows to discover the presence of a large void inclusion, [17], [22]. PD measurements performed on calibrated void samples have shown the same behavior, [18], [19], [20], [21].

C. TRANSITION OF PRPD PATTERNS
The influence of voltage conditioning on new insulation systems was also investigated. Some new coils were subjected to a constant voltage for a long time to evaluate the time behavior of the PRPD patterns during the initial voltage conditioning. Some significant patterns recorded by testing a coil insulated with a PTI-1 system and supplied with a constant voltage of 6.34 kV, are shown in Figure 6.
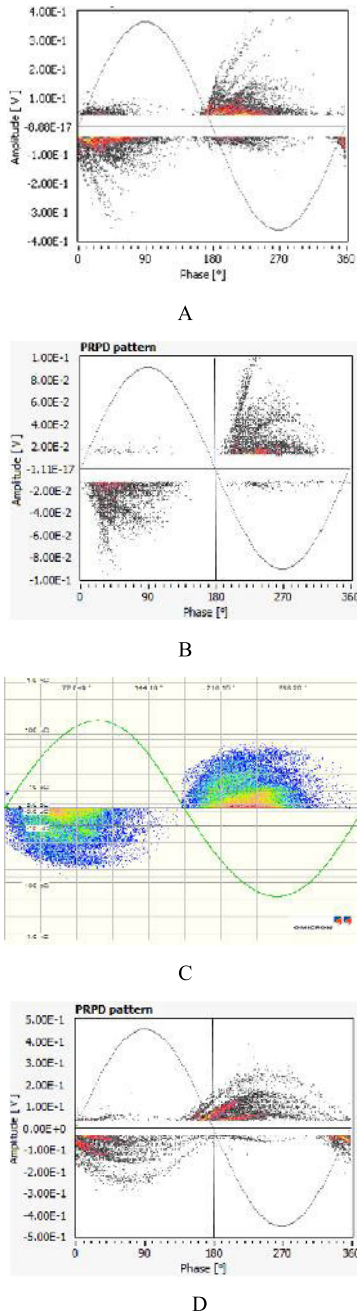
A

B

C

D

FIGURE 4. Examples of PRPD patterns recorded testing coils at 6.38 kV (phase-to-ground); (A) and (B) patterns relevant to the same coil insulated using the PTI-2 technology, obtained using two different commercial PD instruments; (C) pattern relevant to a coil insulated with PTI-1 technology; (D) a single phase of a 10kV complete stator of an induction motor insulated with FLT technology.

Initially, streamer-like discharges occurred within the larger voids, resulting in a characteristic pattern composed of stripes with higher discharges (Fig.6A. See also Fig.1).

These discharges progressively modify both the embedded gas and void surface, thus reducing the PD activity. Figs 6B and 6C show PRPD patterns recorded after 30 and 60 min, respectively. As can be seen, the higher-amplitude discharges

A

B
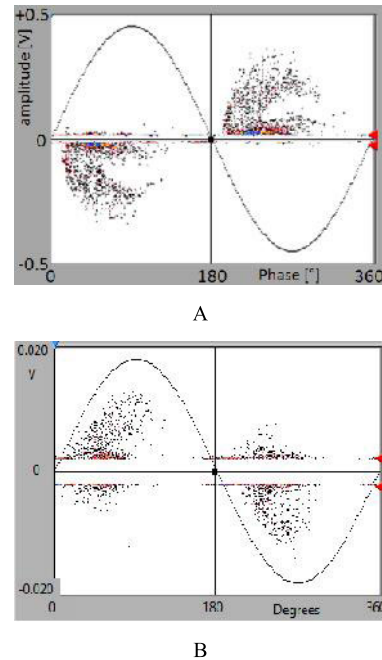
FIGURE 5. Examples of PRPD patterns recorded at 6.36 kV, due to macro-voids recorded on a new coil using (A) a C_k = 1nF and (B) a HFCT (PTI-1 insulation technology).

tend to extinguish, and the shape of the PRPD patterns appears more rounded.

After approximately 2 h, the higher discharges disappeared, and the PRPD pattern appeared rounded and symmetric with respect to the voltage polarity (Fig.6D). This result is in agreement with those obtained by testing simulated cavities [20], [21].

D. INSULATION SYSTEMS IN ALMOST STEADY-STATE CONDITIONS

After a period of voltage conditioning, whose duration depends on the applied voltage, insulation technology, and impregnation resin, the amplitude of the discharges tend to decrease and the "stripes" of higher PD tend to progressively disappear and remain only a rounded-shaped PRPD pattern, symmetric in both voltage polarities. Figure 7 shows some examples of PRPD patterns due to distributed microvoid PD in the insulation under almost steady-state conditions. In particular, Fig.7A shows a pattern obtained by testing at 8 kV a Roebel-bar provided by the RR-1 insulation system and inserted in a stator mock-up, [5], [7]. Figs.7B and 7C are obtained by testing two coils at 6.34 kV, whose insulation systems have been realized for the PTI-1 and PTI-2 systems, respectively.

The PRPD pattern recorded by testing a single phase of an induction motor rated at 10 kV, after approximately one year of service, is shown in Fig.7D. The results of the PD tests performed on different coils or machines, new or in service, using different acquisition systems, showed the same behavior. These patterns are in agreement with those presented in Annexes of [2], [3], and [4] for the same typology.
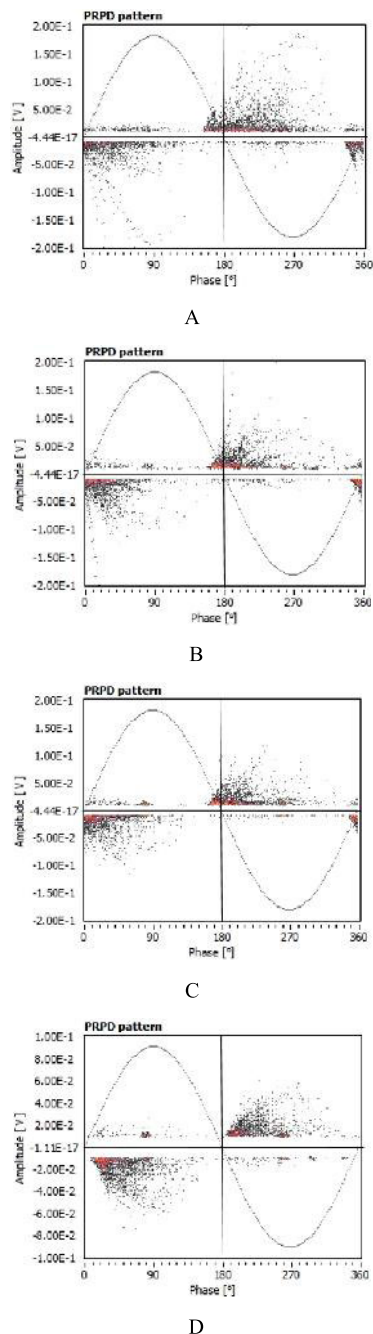
FIGURE 6. Time behavior of the PRPD patterns due to distributed micro voids occurring in a single coil manufactured using an insulation based PTI-1 system. PD acquisition after start of the voltage conditioning at 6.34 kV: A) 5 min.; B) 30 min.; C) 60 min.; D) 120 min.
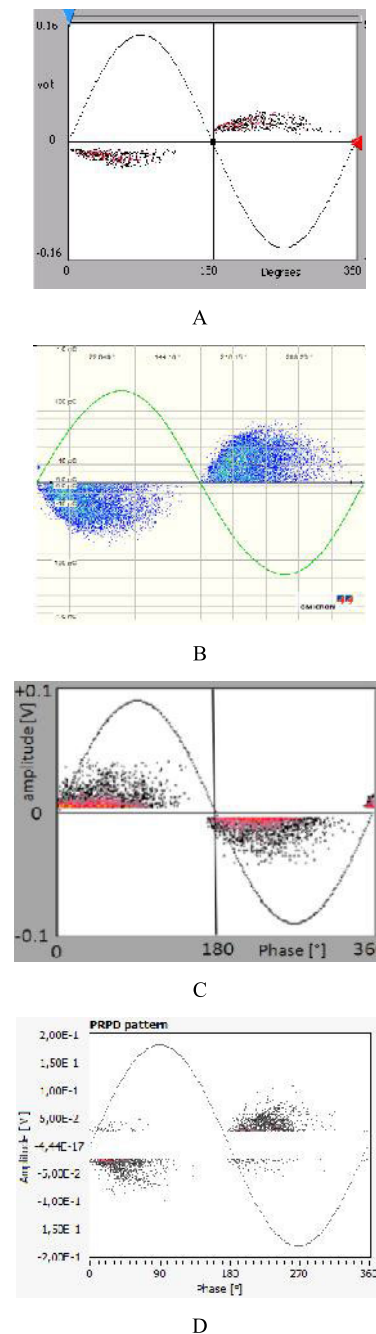

FIGURE 7. Examples of PRPD patterns due to distributed micro-voids in almost steady-state conditions. A) bar with RR-1 insulation tested at 8kV; B) and C) VPI coils tested at 6.34kV and insulated with PTI-1 and PTI-2 technology, respectively. PD tests performed using two different instruments; D) pattern obtained testing a single phase of an induction motor rated 10 kV after about one year of service; FLT insulation system.

It is must be point out that during a conditioning period, it was observed a PD amplitude reduction of 3-4 times. The discharge transition can constitute a problem when the pass/fail criterion is based on PD amplitude threshold levels. If the threshold is established considering almost steady-state conditions, tests performed on the new insulation can fail.

In contrast, acceptance tests based on higher threshold levels that consider discharge amplitudes in new insulation can pass even in the presence of PD owing to different types of defects having a discharge amplitude below this high threshold level.

V. PRPD PATTERNS OF DIFFERENT DEFECT TYPOLOGIES
Owing to the different charge mobility in the positive/negative half-cycles of the applied voltage, the PRPD

patterns exhibit higher discharges in positive/negative voltage polarities if the defects are close to high-voltage (copper conductor) or low-voltage electrodes (stator core), and they appear symmetric if the defect is surrounded by insulation. Thus, the pulse signals are defined as positive/negative if they occur in the positive/negative half-cycles of the applied voltage. This definition presents the great advantage of being connected with the original cause of the discharges (the electric field distribution as a consequence of the voltage application) and does not depend on the direct/indirect connections of the test circuit [1], the type of coupler (coupling capacitor, HFCT, antenna probe), and voltage- or current-type signal pulses.

The shapes of the PRPD patterns were intuitively analyzed using the visual inspection approach (rule B, Cap.III).

A. TAPE DELAMINATION

Tape delamination is typically caused by poor manufacturing as well as thermo-mechanical stress during machine service. In general, it consists of a flat cavity surrounded by tapes or impregnation resin owing to detachment between the tape layers (internal tape delamination). Discharges occurring in flat cavities artificially or "naturally" created generate patterns with triangular shapes that are symmetric with respect to the voltage polarity, similar to those reported in Figure 8. In particular, the PRPD pattern recorded by testing a Roebel bar provided with the RR-2 system at 8 kV is shown in Fig.8A, whereas that obtained by testing a VPI coil at 7.5 kV completed with FLT insulation is shown in Fig.8B. Two different commercial PD instruments connected to $C_k = 1nF$ and $C_k = 80pF$ were used in the setup for the former and latter PD tests, respectively. These shapes are in agreement with those reported in the annexes in [2] and [3]. If the flat cavities tend to extend in the longitudinal direction (parallel to the HV and LV electrodes), the repetition rate of the higher amplitude discharges tends to increase, but the shape of the relevant PRPD patterns always remains triangular and symmetric in voltage polarity, [13], [14].

B. CONDUCTOR-SIDE DELAMINATION

The PRPD patterns recorded in the presence of a flat cavity due to copper conductor-insulation detachment show an asymmetric half-pattern, triangular shaped with higher amplitude discharges in the positive half-cycle of the applied voltage (positive dominant polarity). Two typical examples are shown in Figure 9. Fig.9A shows the PRPD pattern obtained by testing a coil insulated with PTI-1 type, provided by the artificial conductor delamination at 6.38 kV, using an HFCT. Figure 9B shows a conductor delamination discovered during on-line PD tests on a hydro generator equipped with VPI coils at a phase-to-ground rated voltage of 9.49 kV and full load ($C_k = 80pF$). This behavior can be explained by the fact that charges can move easily from the conductors to the insulation surface, whereas less mobility characterizes the
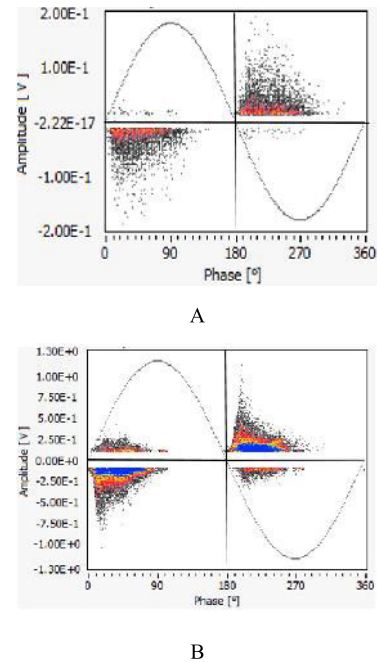

FIGURE 8. Examples of PRPD patterns due to internal delamination. PD tests performed on A) a RR-2 bar at 8kV and B) FLT, VPI coil for a large hydrogenerator at 7.5 kV.

charge movement from the insulation surface to the conductors.

During the evolution of the discharge site, the patterns remained triangular in the positive half-cycle of the applied voltage. These patterns are in agreement with those reported in the Annexes of Standards, [2], [3], [4].

C. CSC DETERIORATION/DETACHMENT

The synergic effect of mechanical and thermal stresses can induce deterioration (with coil detachment in GVPI insulation) of the conductive tape or varnish that constitutes the CSC. This defect can incept the so-called slot discharges. The typical PRPD patterns generally associated with slot discharges show a dominant polarity in the negative half-cycle of the applied voltage, having triangular or trapezoidal, left-skewed shapes (see e.g., reference patterns in Annexes of [2], [3], [4]). These patterns can be explained in terms of the different charge mobilities. The stator core can supply a discharge process with a significant amount of charge in the negative half-cycle of the applied voltage. At the opposite voltage polarity, owing to the deteriorated conductive CSC, few charges can be collected from the coil/bar surface; thus, the PRPD pattern shows both a lower amplitude and repetition rate.

Figure 10 reports two examples of PRPD patterns due to slot discharges.

That shown in Fig.10A has been recorded testing a Roebel bar whose main insulation is based on RR-1 insulation system, inserted in a stator mock-up ([7], [13]) where the varnished CSC was abraded to generate slot PD. Test voltage
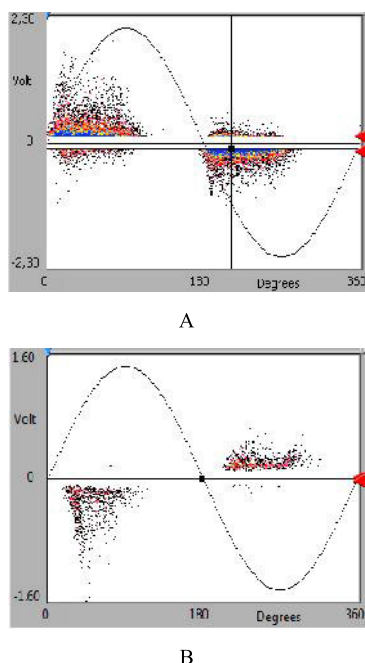
FIGURE 9. Examples of PRPD patterns due to conductor delamination. Tests performed on (A) a coil insulated with PTI-1 type and provided by an artificial defect at 6.38 kV; B) on a hydrogenerator at rated voltage of 16 kV and 160 MVA at full load.
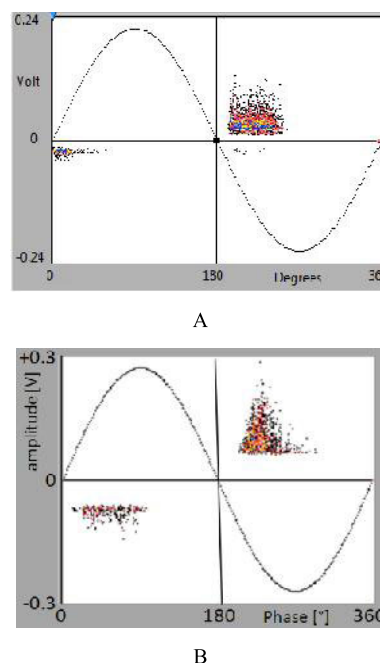

FIGURE 10. Examples of PRPD patterns recorded testing (A) a Roebel bar with abrasion of the CSC varnish. PD tests at 8kV using a Ck=1nF; B) a VPI, FLT insulated coil during a multifactor ageing test, at 6.38 kV, using a Ck=500pF.

was of 8 kV and data was recorded using a $C_k = 1nF$. The trapezoidal shape of the negative half-pattern, left skewed, is evident. Figure 10B shows a pattern recorded during multifactor aging tests of VPI coils insulated with FLT technology (6 days of electric stress at rated voltage and 22.6% overheating followed by 3 h of mechanical vibrations). The magnetic core was simulated using two L-shaped metallic profiles taped with thermosetting tape and grounded. The coils were tested after each aging cycle. After several cycles, in one coil, a triangular pattern appeared in the negative half-cycle of the applied voltage [14]. The pattern in Fig.10B refers to an applied voltage of 6.38 kV (phase-to-ground) using $C_k = 500pF$. At the end of the experiment, the presence of delamination between the coil and L profile was verified by opening the two L-profiles. This result shows that the deterioration of taped or varnished CSC can generate similar patterns.

D. DETERIORATION OF SCC
In coils/bars rated 6-7 kV and above, external SCC are provided at the edges of the CSC to reduce the electric field below the PD inception level. For GVPI technology, SCC is based on polymeric SiC tapes, while varnished coatings are also used in VPI insulation for larger machines or Roebel bars.

Different stresses can deteriorate SCC in different ways. The most common PRPD pattern due to SCC deterioration is characterized by a rounded or triangular shape, right-skewed with respect to the voltage phase with a discharge predominance in the negative half-cycle of the applied voltage (see

e.g., Annexes of [2], [3], [4]). Figure 11 shows the PRPD patterns recorded by testing a Roebel bar rated 15 kV with a deteriorated SCC varnish at different voltage levels using an HFCT. Figures 11A and 11B show the PRPD patterns recorded at 8 and 13 kV, respectively. Using an acoustic device, it was found that below 9 kV, discharges occurred in a localized area above the SCC side, whereas above 9 kV, discharges were found around both sides of the SCC at the edges of the CSC. It is likely that the weakening of the varnished SCC did not result in an electric field below the PD inception voltage. As can be seen, the pattern in Fig.11A is similar to that reported in Annexes [2], [3], [4] for the same defect topology, whereas that of Fig.12B has not been considered in the Annexes.

During the periodical PD tests performed after the aging cycles of a set of coils insulated with FLT technology and provided by taped SCC (6 days of electric stress at rated voltage and 22.6% overheating followed by 3 h of mechanical vibrations), tape detachment was observed in one coil, whereas in another coil, the thermal shrinkage generated a large void below the SCC tape. Examples of the PRPD patterns recorded by testing these two coils at a rated voltage of 6.36 kV, are shown in Figure 12. Discharges inside the tape delamination generated a PRPD pattern with a triangular shape, symmetric with respect to the voltage polarity (Fig.12A), very similar to those associated with internal delamination (see Fig.8), while Fig.12B reports the PRPD pattern recorded by testing the coil with the bumped SCC tape. As can be seen, this pattern recalls
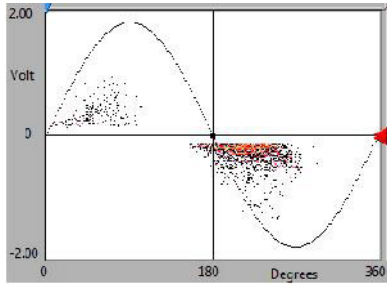
A
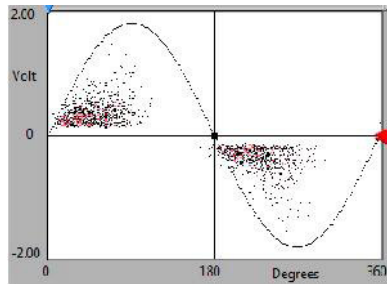
B

FIGURE 11. Examples of PRPD patterns recorded testing a single bar whose SCC was abraded to generate surface PD. A) pattern generated by discharges in the abraded area; B) pattern due the weakining of the whole SCC.

A

B

FIGURE 12. Examples of PRPD patterns due to CSC tape detachment. A) Coil-SiC tape delamination; B) SiC tape shrinkage.

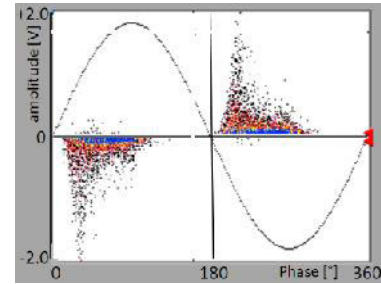those generated by internal macro-voids (see Fig.5). Again, these cases were not considered in the Annexes [2], [3], [4].

These examples clearly show that the shapes of the PRPD patterns can differ if the SCC is varnished or taped, and that different stresses can deteriorate the taped SCC in different ways, thus generating different PRPD patterns.
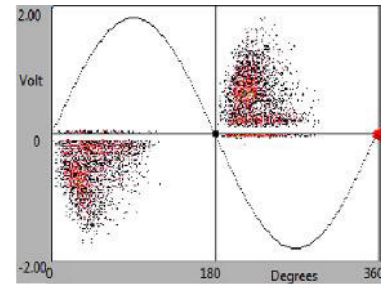
E. COILS WITHOUT SCC

Coils designed in a voltage range of 4-7 kV are typically manufactured with CSC, but cannot be equipped with SCC. Coils rated at 6 kV (not provided by the SCC tape) were tested at different voltage levels. Surface discharges incepted at the edges of the CSC tape (visualized using an optical device) were recorded starting from 3.5 kV. All PRPD patterns show a triangular shape, left-skewed, and symmetric in voltage polarity, as shown in Figure 13. Figs.13A and 13 B are relevant to the PD tests performed at 4 kV and 6.6 kV, respectively, using Ck=1nF. As can be seen, these patterns are similar to those associated to internal tape delamination and SCC tape delamination (see Fig.8 and Fig.12A, respectively).

F. AIR-GAP DISCHARGES

One of the effects of mechanical vibrations in service is the possible reduction in the space between the bars/coils of different phases in the overhang or the adjacent metallic tooth that compresses the magnetic core. Because of the different dielectric constants (insulation and air), the electric field in the air gap can be enhanced above the PD inception voltage. Figure 14 shows two examples of air-gap discharges. In particular, Fig.14A shows the PD tests performed to eval-

uate coils inserted in a mock-up, provided with PTI-1 type insulation. The surfaces of these coils were protected using polyester tape. Fig.14B shows two Roebel bars provided by RR-1 insulation, positioned one on top of the other to incept air-gap discharges.

As can be seen, both examples present discharges having more or less, the same amplitude and their shape are similar to those commonly indicated in literature as ''bar-to-bar'' or ''bar-to-finger'' PD, [2], [3], [4]. Discharges in the air gap between the two different phases show a similar PRPD shape but a shifted forward/delay of 30°.

G. SURFACE TRACKING

Surface tracking was reproduced by positioning a metallic needle on the surface of a coil and connecting it first with the conductor and then with the LV electrode.

The test voltage was increased with the inception of surface discharges (approximately 6.5 kV in addition to the internal PD). Figure 15 shows examples of tracking discharges with the needle connected to the HV (Fig.15A) and the LV electrode (Fig.15B) of a FLT insulated coil. The applied voltage was 7.2 kV in both cases and $C_k = 1nF$ was used in this test. These patterns appear elongated in width and are concentrated in a short range of phases of the applied voltage.

VI. APPLICATION EXAMPLES

The proposed pass/fail criterion was applied to evaluate the quality of different insulation systems of bars, coils, and complete machines, both in the laboratory and factory. Because distributed micro-void PD are always present, separation techniques are required very often.
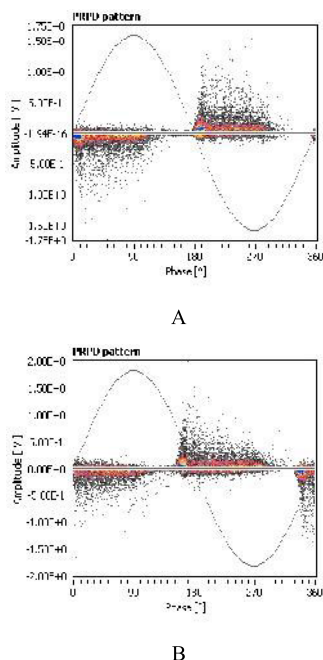
A

B

FIGURE 13. Examples of PRPD pattern due to surface discharges occurring at the edges of the slot conductive tape on a coil not provided by the outer SCC. Tests performed at A) 4 kV and B) 6.6 kV.
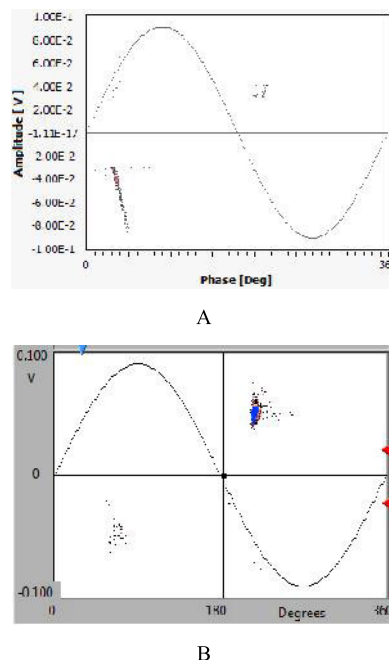

A

B

FIGURE 15. Examples of PRPD patterns recorded testing (A) 6.6kV coil having a needle tip connected to the HV electrode and (B) a 15kV coil with a surface tracking generated on the CSC surface, during a voltage endurance test. Test voltage of 7.2kV and 9kV for PD patterns (A) and (B), respectively.
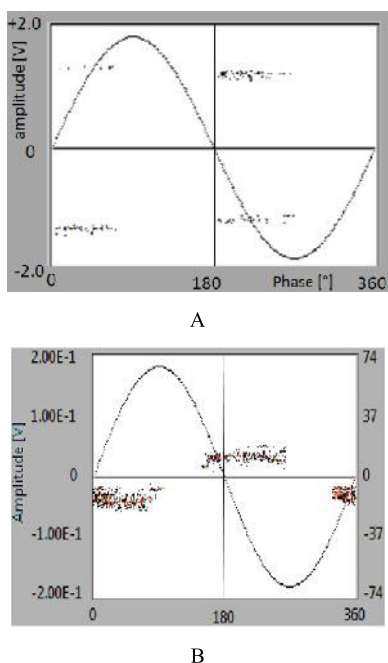

A

B

FIGURE 14. Examples of PRPD patterns due to gap type discharges in air: A) between two coils (PTI-1 main insulation); B) between two RR-1 bars.

In addition to the shape analysis of the PRPD patterns, the significant role played by the separation map in the procedure is evident from the discussion of the following examples. In fact, the comparison of the shape of the additional sub-patterns with those proposed as a reference in the

previous chapters allowed the discovery of defective components that may lead to the failure of the proposed test.

A. COIL WITH SURFACE PD
Figure 16 shows an example of the application of this procedure to qualify an insulation system based on FLT technology. Coils designed for a rated voltage of 11 kV were inserted into a mock-up to evaluate the impregnation quality. PD tests were performed in the laboratory from 5 kV to 11 kV with steps of 1 kV using $C_k = 1$ nF. A new discharge phenomenon was observed at a voltage of 7 kV.

The experimental PRPD pattern recorded at 8 kV is shown in Fig.16A. The presence of these two groups in the separation map in Fig.16B is evident.

The shape of the sub-patterns obtained after the separation clearly addresses the distributed micro-void PD (Fig.16C is associated with the white group in Fig.16B). Compare this sub-pattern with those reported, for example, in Fig.1. Fig.16D associated with the red group in Fig.16B, addresses to slot discharges (see Fig.10A).

The result does not meet the defined acceptance criteria. It was found that owing to the poor insertion of one coil, the impregnation resin did not completely fill the CSC and slot wall.

B. INSULATION BREAKDOWN IN A STATOR WINDING
Offline PD tests were performed in a factory to verify the conditions of the stator of an induction motor rated at 11 kV. PD tests were performed in each phase using $C_k = 500$pF.
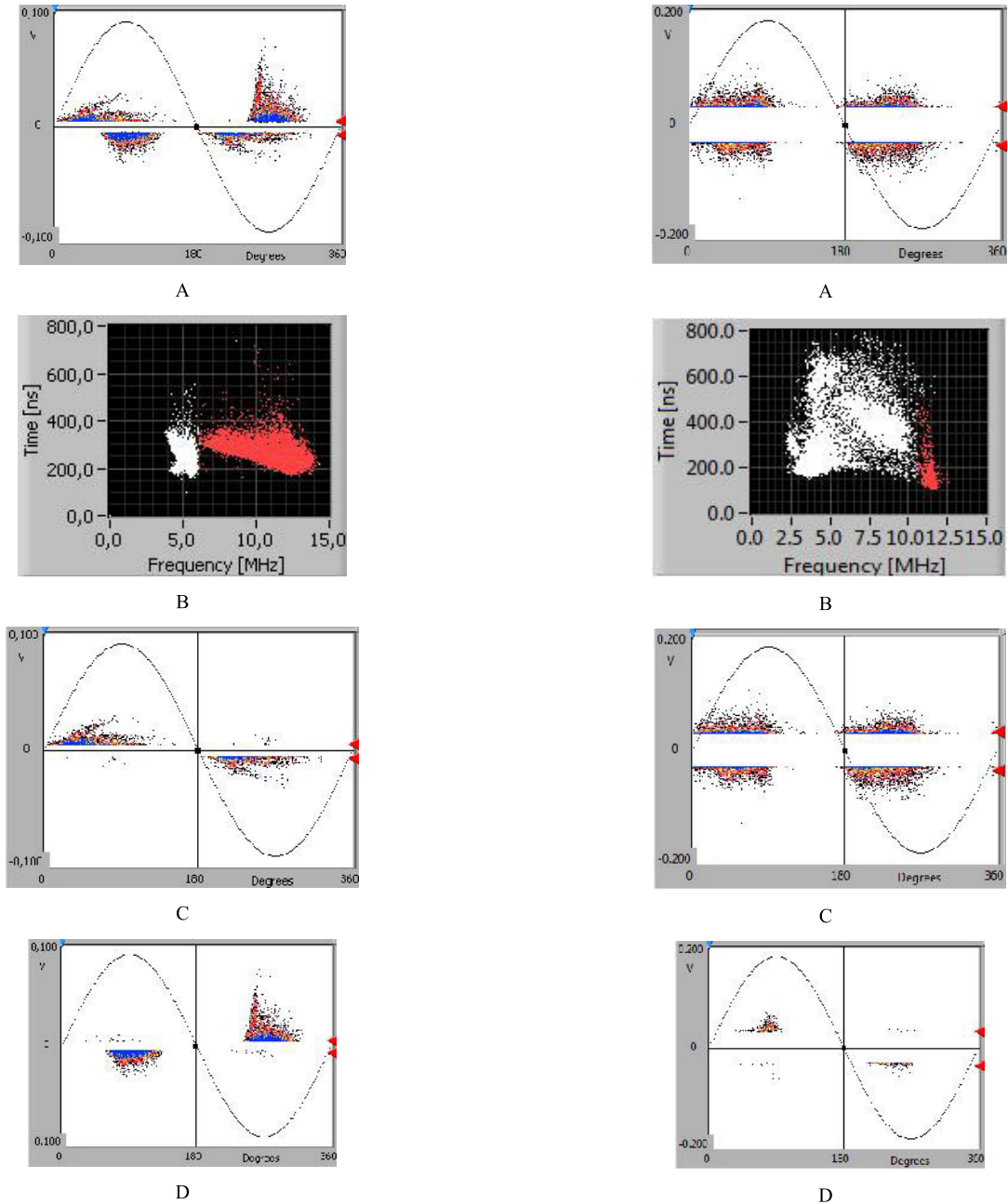
A

B

C

D

FIGURE 16. PRPD pattern recorded testing a coil for GVPI induction motors at 8 kV. A) the experimental PD pattern; B) the separation map; C) and D) the sub-patterns relevant to groups white and red in the map of Fig.16B.

A

B

C

D

FIGURE 17. Experimental PRPD pattern recorded at 5 kV (A) with the relevant separation map (B). C) and D, sub-patterns associated to white and red groups of signals of the TF map of Fig.17B, respectively.

The PD inception voltage was about 3.4 kV – 3.6 kV for all phases. During the transition between 5 and 6 kV, a breakdown occurred at the edge of the CSC of a phase. The PRPD pattern recorded at 5 kV before breakdown is shown in Figure 17A with the relevant separation map (Fig.17B). Separation provided two distinct groups: white and red in the range of 2.5-10 MHz and 10-12.5 MH, respectively. The white group is composed by three sub-groups partially overlapped. The sub-patterns associated to these three groups show a rounded shape, symmetric in polarity as those asso-

ciated to distributed micro-void PD in almost steady-state conditions. In this paper, they are merged in a single PRPD pattern (Figure 17C). The PRPD shape is still rounded and symmetric in voltage polarity that maintain the diagnostic information (compare Figures 17C and e.g., Figure 7).

The shape analysis of the sub-pattern associated to the red cluster in the TF map (frequency range of 11-12 MHz) shows a dominant PD polarity in the positive half-cycle of the applied voltage, well separated by the main group of signals (white group in Figure 17B). The relevant sub-pattern,
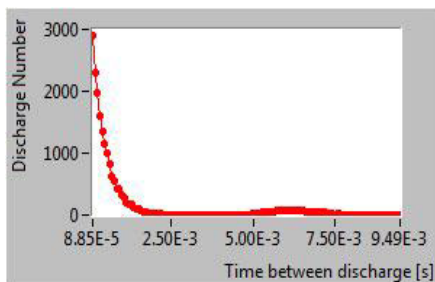
A
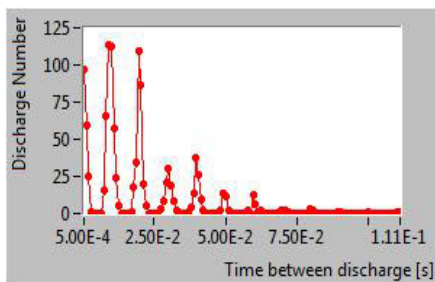
B

FIGURE 18. Histograms of the inter-time distributions of consecutive PD signals relevant to the sub-patterns of Fig.17C (A) and Fig.17D (B), respectively.

reported in Fig.17D, shows a dominant PD polarity in the positive half-cycle of the applied voltage, thus indicating discharges occurring close to the conductors (Fig.9, Par.B, Cap.V).

The inter-time distributions between two consecutive discharges, relevant to the sub-patterns of Fig.17C and 17D, are shown in Figure 18. The distribution of Fig.18B, associated with the sub-pattern of Fig.17D, shows the typical signature of an electrical tree, as demonstrated in [23], while the histogram of Fig.18A associated with the distributed micro-void PD in Fig.17C, appears regular. This example demonstrates that higher discharges are not necessarily the most dangerous. Without pulse-signal separation and shape analysis of the PRPD, this result cannot be achieved.

C. PD TEST ON A VPI COIL

This example refers to the application procedure to qualify a FLT insulation system provided by a varnished CSC and SCC and designed for a VPI coil with a rated voltage of 15 kV. Figure 19 shows the test result obtained by applying 8.67 kV, using $C_k = 1nF$ as the coupler. The experimental pattern is shown in Fig.19A and the relevant TF map is shown in Fig.19B. Figures 19C and 19D show the black and red groups of the TF in Fig.19B. The sub-pattern of Fig.19C is associated with distributed micro-voids of the new insulation (see e.g., Figures 1 or 3), while the PRPD of Fig.19D, triangular shaped, symmetric in voltage polarity can be associated with internal delamination (compare this sub-pattern with those reported in Fig.8). Again, this result cannot be achieved without the support of a separation map.
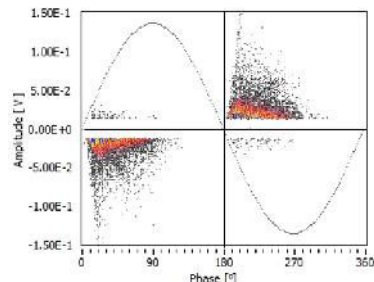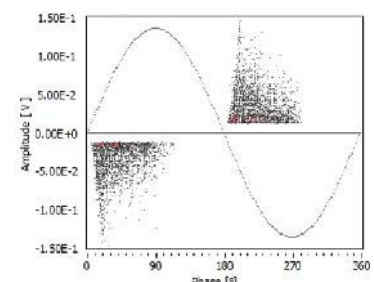

A
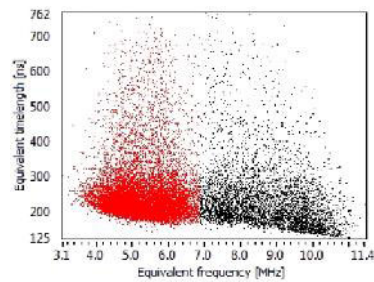
B
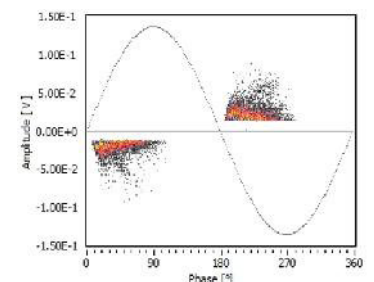
C

D

FIGURE 19. Result of a PD acquisition obtained testing a VPI coil at 8.67 kV, using a $C_k = 1$ nF. A) the experimental PRPD patterns and B) the relevant TF map. C) and D) the sub-patterns relevant to groups white and red of the TF map (Fig.20B).

Even this test does not meet the defined acceptance criteria. The pressing and heating parameters were modified to obtain a better impregnation quality.

D. OFF-LINE PD TEST ON A SYNCHRONOUS GENERATOR

The last example belongs to a set of PD acquisitions performed during offline tests of a single phase of a synchronous generator, whereas the other phases are grounded. The
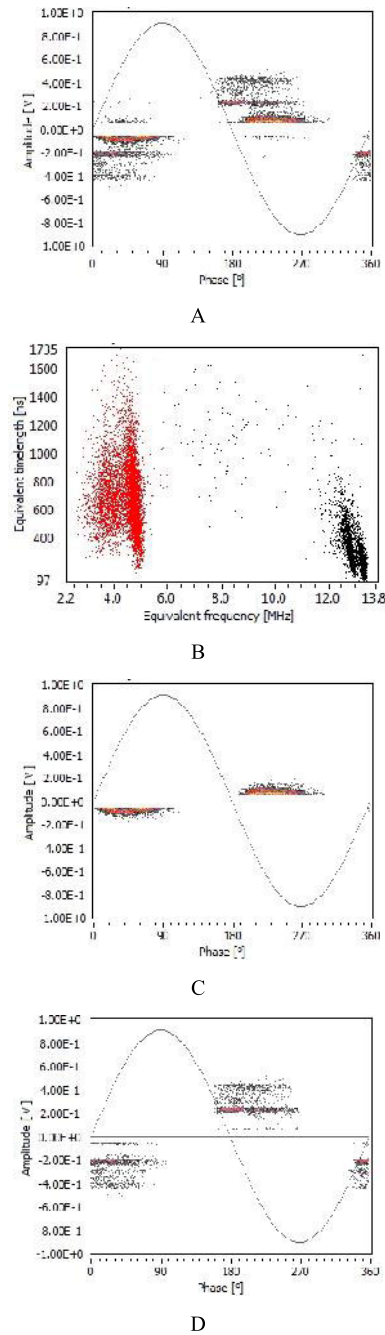
FIGURE 20. Result of a PD acquisition obtained testing off-line a synchronous generator at 10 kV, using a C_k = 2 nF. A) the experimental PRPD patterns and B) the relevant TF map. C) and D) the sub-patterns relevant to groups white and red of the TF map (Fig.20B).

insulation system was based on another type of RR technology, completed with a varnished CSC and SCC, and designed for a rated voltage of 18 kV. Tests were performed during a periodic check of the generator, after ten years of service.

Figure 20 reports the PD test results obtained at 10 kV using a C_k = 2nF. The experimental pattern is shown in Fig.20A and the relevant TF map is reported in Fig.20B.

Figures 20C and 20D are relevant to groups black and red of the TF of Fig.20B.

As can be seen, the sub-pattern of Fig.20C shows rounded and symmetrical PRPD patterns, which can be associated with distributed micro-void PD in almost steady-state conditions (again, see e.g., Figures 1 or 3).

The shape of the PRPD in Fig.20D is composed of stripes of discharges having more or less the same amplitude, similar to those associated with air-gap discharges (see Fig.14). Even in this example, the result does not meet the defined acceptance criteria. An inspection of the stator end-windings brought to evidence discharges between the bar surface and the stator-core pressure-finger.

VII. CONCLUSION
A new criterion for acceptance tests and condition assessment of insulation systems of AC rotating machines based on shape analysis of PRPD patterns is proposed in this paper. It has been assumed that the insulation is in good condition when it is affected by distributed microvoid PD, and no other PRPD patterns are detected during the test. Distributed microvoid PD present two typical shapes relevant to new and almost steady-state insulation systems, which are different from those due to other defect typologies and are thus easily distinguishable. The presence of patterns with different shapes causes the failure of the test. The use of a separation map is strongly suggested to demonstrate that no other discharge phenomena due to different types of defects are active.

The defective component can be identified by comparing the separated pattern with those reported in Cap.V used as a reference. The number of PRPD patterns presented in this paper is more than those reported in the Annexes of the actual standards and differences. The general validity of the proposed method has been empirically verified using different PD instruments connected to different couplers, thus obtaining measurement systems with different gains and bandwidths. Additional investigations are still necessary to confirm this result.

It can be concluded that the shape analysis of the PRPD patterns obtained by the analysis of a separation map seems promising to overcome the problems caused by the use of acceptance tests based on PD amplitude threshold levels.

REFERENCES
[1] *IEC Partial Discharge Measurements*, IEC Standard 60270-2000, Apr. 2001.

[2] *Guide to the Measurements of Partial Discharges in Rotating Machinery*, IEEE Standard 1434-2000, 2000.

[3] *Rotating Electrical Machines: Partial Discharge Off-line Measurements on the Stator Winding Insulation of Rotating Machinery*, IEC/TS Standard 60034-27-1, Dec. 2006.

[4] *Rotating Electrical Machines: On-Line Partial Discharge Measurements on the Stator Winding Insulation of Rotating Electrical Machines*, IEC/TS Standard 60034-27-2, 2012.

[5] A. Contin, A. Cavallini, G. C. Montanari, C. Hudon, M. Belec, and D. N. Nguyen, "Searching for indexes suitable for rotating machines diagnosis," in *Proc. Conf. Rec. IEEE Int. Symp. Electr. Insul.*, Jun. 2006, pp. 101–105.

[6] A. Petit, "Comparison of PD amplitudes of stator bars taken with different instruments," in *Proc. IEEE Electr. Insul. Conf. (EIC)*, Jun. 2015, pp. 255–261.

[7] C. Hudon and M. Belec, "Partial discharge signal interpretation for generator diagnostics," *IEEE Trans. Dielectr. Electr. Insul.*, vol. 12, no. 2, pp. 297–319, Apr. 2005.

[8] A. Cavallini, A. Contin, G. C. Montanari, and F. Puletti, "Application of a new methodology for identification of PD in electrical apparatus," *IEEE Trans. Dielectr. Electr. Insul.*, vol. 12, pp. 203–215, Apr. 2005.

[9] W. Koltunowicz and R. Plath, "Synchronous multi-channel PD measurements," *IEEE Trans. Dielectr. Electr. Insul.*, vol. 15, no. 6, pp. 1715–1723, Dec. 2008.

[10] L. Hao, P. L. Lewin, J. A. Hunter, D. J. Swaffield, A. Contin, C. Walton, and M. Michel, "Discrimination of multiple PD sources using wavelet decomposition and principal component analysis," *IEEE Trans. Dielectr. Electr. Insul.*, vol. 18, no. 5, pp. 1702–1711, Oct. 2011.

[11] A. Contin and S. Pastore, "Classification and separation of partial discharge signals by means of their auto-correlation function evaluation," *IEEE Trans. Dielectr. Electr. Insul.*, vol. 16, no. 6, pp. 1609–1622, Dec. 2009.

[12] A. Cavallini, A. Contin, G. C. Montanari, and F. Puletti, "Advanced PD inference in on-field measurements. I. Noise rejection," *IEEE Trans. Dielectr. Electr. Insul.*, vol. 10, no. 2, pp. 216–224, Apr. 2003.

[13] G. Rabach, A. Contin, F. Razza, and M. Visintin, "On turbogenerator HV stator winding condition assessment by the analysis of PDHD detected on phases and insulated coils after untimely failure," in *Proc. 6th IEEE-ICDS*, Jun. 1998, pp. 185–188.

[14] A. Contin, M. Aizza, F. Fantin, and A. Piccolo, "Identification of PD sources and insulation technologies in rotating machines," in *Proc. IEEE Electr. Insul. Conf. (EIC)*, Jun. 2015, pp. 458–462.

[15] R. Candela and A. Contin, "A portable instrument for the location and identification of defects generating PD," in *Proc. Electr. Insul. Conf. (EIC).*, Jun. 2011, pp. 469–473.

[16] G. C. Stone, I. Culbert, H. Dirani, and A. Boulter, *Electrical Insulation for Rotating Machines*. Piscataway, NJ, USA: IEEE Press, 2004.

[17] M. Piller, G. Schena, A. Contin, and G. Rabach, "Ground-wall insulation system analysis combining advanced imaging techniques and numerical simulation," *Electr. Power Syst. Res.*, vol. 116, pp. 444–450, Nov. 2014.

[18] C. Hudon, R. Bartnikas, and M. R. Wertheimer, "Spark-to-glow discharge transition due to increased surface conductivity on epoxy resin specimens," *IEEE Trans. Electr. Insul.*, vol. 28, no. 1, pp. 1–8, Feb. 1993.

[19] P. Morshuis, "Assessment of dielectric degradation by ultrawide-band PD detection," *IEEE Trans. Dielectr. Electr. Insul.*, vol. 2, no. 5, pp. 744–760, Oct. 1995.

[20] F. Gutfleisch and L. Niemeyer, "Measurement and simulation of PD in epoxy voids," *IEEE Trans. Dielectr. Electr. Insul.*, vol. 2, no. 5, pp. 729–743, Oct. 1995.

[21] K. Nakao, T. Kondo, Y. Suzuoki, and T. Mizutani, "Φ-q-n patterns and current shapes of partial discharges in voids," in *Proc. Int. Symp. Electr. Insulating Mater.*, 1998, pp. 665–668.

[22] A. Contin, M. Piller, and G. Schena, "Analysis of 3D computed tomographic imaging of ground-wall insulation for AC rotating machines," *IEEE Trans. Dielectr. Electr. Insul.*, vol. 22, no. 3, pp. 1520–1529, Jun. 2015.

[23] A. Cavallini, M. Conti, G. C. Montanari, C. Arlotti, and A. Contin, "PD inference for the early detection of electrical treeing in insulation systems," *IEEE Trans. Dielectr. Electr. Insul.*, vol. 11, no. 4, pp. 724–735, Aug. 2004.

ALFREDO CONTIN (Life Member, IEEE) was the Head of the Department of Engineering and Architecture, University of Trieste, Italy. He is currently an Associate Professor with the Department of Engineering and Architecture, University of Trieste. His fields of interest are characterization, aging, and diagnostics of insulation materials and systems using partial discharges. He is the author or co-author of up to 150 articles. He was a member of IEC CT2/MT10 and CIGRE TF 30/15. He cooperates with different Industries, research Centers, and Universities.

ANDREA PICCOLO was born in Pordenone, Italy, in April 1983. He received the B.Sc. and M.Sc. degrees in electrical engineering from the University of Trieste, Italy, in 2007 and 2010, respectively. He was a Senior Electrical Insulation Engineer with Nidec ASI and Collaborated with Tech Imp and Omicron, Development of Insulation On-Line Monitoring Systems. He is currently a Senior Consultant in electrical machines with DNV-GL Energy. His current interests include quality assurance, remaining life assessment and root cause analysis of electrical machines for oil and gas, marine, and energy applications. His main fields of interest are design, manufacturing and qualification of electrical insulation system, as well diagnostics and reliability of electrical equipment based on the specific applications.

● ● ●